PAPER

Gold cluster–nanoparticle diad systems for plasmonic enhancement of photosensitization

Atsushi Kogo, Yukina Takahashi,† Nobuyuki Sakai‡ and Tetsu Tatsuma*

Quantum-sized gold clusters are deposited on TiO_2 both as a photosensitizer and catalyst, and coupled to plasmonic gold nanoparticles as a light harvesting antenna. Photocurrent enhancement was observed for $Au_{25}(SG)_{18}$ and $Au_{38}(SG)_{24}$ but not for $Au_{102}(SG)_{44}$ (SG = glutathione). The maximum enhancement factor of ~9 is reached at 900 nm.
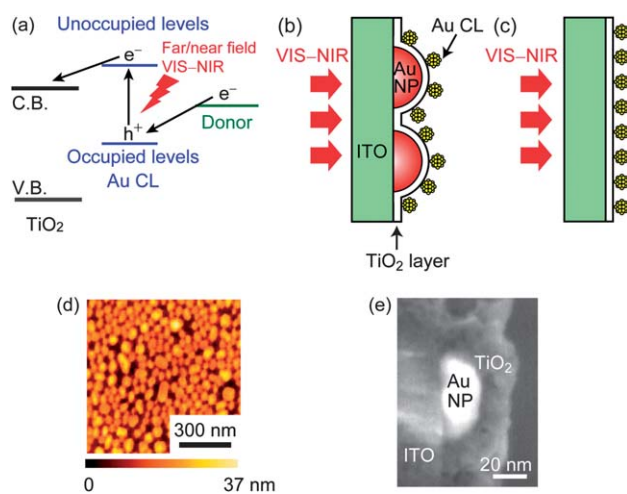
1 Introduction

Quantum-sized metal clusters (CLs), which are smaller than 2 nm in diameter and consist of less than 250 metal atoms, have discrete electron levels and exhibit molecular-like properties rather than bulk metals.[1,2] For example, metal CLs exhibit optical absorption from ultraviolet to near infrared regions,[3,4] fluorescence[5,6] and two photon absorption[7] based on electron transition between the discrete electron levels. Metal CLs supported on an appropriate substrate also work as effective catalysts[8] and electrocatalysts.[9]

Our recent studies have shown that metal CLs serve as a photosensitizer of TiO_2 (Fig. 1a) as do some ruthenium dyes.[10,11] Metal CL-modified TiO_2 exhibits photovoltaic[11–13] and photocatalytic[14] properties in response to visible and near infrared light. The metal CLs have a great advantage as a sensitizer; their HOMO–LUMO energy gap and absorption wavelength can be tuned by changing their core size.[3,15] Moreover, efficient redox reactions can be expected if the catalytic and electrocatalytic properties of the CLs are combined with their capability as a sensitizer.

Despite the high internal quantum efficiency of ~60% for Au CL-modified TiO_2, their external quantum efficiency (incident photon-to-electron conversion efficiency, IPCE) has been as low as ~10%.[12] This is due to the low photoabsorption efficiency of the Au CLs (molar absorption coefficient $\varepsilon \sim 10^4$ M^{-1} cm^{-1} at 670 nm).[3] Although the photoabsorption improves as the amount of the Au CLs adsorbed on porous TiO_2 increases, the CLs, which are relatively bulky compared to ruthenium dyes, block the mass transfer of a redox species in the nanopores and the internal resistance would be increased.

In the present work, we couple Au CLs to gold nanoparticles (Au NPs) as a light-harvesting antenna, in order to achieve both high internal quantum efficiency and high photoabsorption. Plasmonic metal NPs, which are larger than 3 nm in diameter, exhibit intense light absorption at a specific wavelength based on localized surface plasmon resonance (LSPR) and generate an optical near field (localized oscillating electric field) around their surface, which in turn excites dyes and semiconductors in the vicinity. Their absorption cross-section usually exceeds their geometrical cross-section[16] and the lifetime of the near field is much longer than the time for photons to pass by a NP. Photons are thus confined in the vicinity of the NPs and photoabsorption of the dyes and semiconductors around the NPs is enhanced. Therefore, the plasmonic metal NPs have been applied to photo-antennas for surface enhanced Raman spectroscopy (SERS),[17] enhanced fluorescence,[18] photocatalysis[19–22] and photovoltaics.[23–25]

Here we report the Au CL–NP diad systems with photocurrents enhanced by a factor of ~6 and ~9 under visible and near

Institute of Industrial Science, The University of Tokyo, 4-6-1 Komaba, Meguro-ku, Tokyo 153-8505, Japan. E-mail: tatsuma@iis.u-tokyo.ac.jp; Fax: +81-3-5452-6338; Tel: +81-3-5452-6336

† Present address: Department of Applied Chemistry, Faculty of Engineering, Kyushu University, 744 Moto-oka, Nishi-ku, Fukuoka 819-0395, Japan.

‡ Present address: International Center for Materials Nanoarchitectonics, National Institute for Materials Science, 1-1 Namiki, Tsukuba, Ibaraki 305-0044, Japan.

Fig. 1 (a) Photocurrent generation at the Au CL-modified TiO_2. Schematic illustration of (b) ITO/Au NP/TiO_2/Au CL and (c) ITO/TiO_2/Au CL electrodes. (d) An AFM image of Au NPs on ITO and (e) a SEM cross-sectional image of an ITO/Au NP/TiO_2/Au CL electrode.

infrared light, respectively. We also found that the enhancement factor is increased as the CL size decreases.

The diad systems with high internal quantum efficiency and intense light absorption, which are characteristic of Au CLs and Au NPs, respectively, would lead to the development of more sophisticated photofunctional devices and materials than conventional CL-based photovoltaics[11–13] and photocatalysts[14] and plasmonic NP-based photovoltaic,[26–28] photocatalytic,[26,29,30] photochromic[31–34] and organic photomorphing[35] materials.

2 Experimental

Synthesis of $Au_{25}(SG)_{18}$

$Au_{25}(SG)_{18}$ (GSH = glutathione) was synthesized according to the literature[3,36] with some modifications. GSH (1 mmol) was added to a methanol solution of $HAuCl_4$ (5 mM, 50 mL). The solution was cooled at 4 °C for 30 min and an ice-cold aqueous $NaBH_4$ (0.2 M, 12.5 mL) was added to the solution under vigorous stirring and aged for 1 h. The precipitate formed was collected by centrifugation (3000g, 5 min) and thoroughly rinsed with methanol and dried in a vacuum at room temperature to obtain a mixture of Au CLs. The mixture (5 mg) was dissolved in an aqueous solution (7 mL) containing GSH (130.7 mg) and stirred at 55 °C under air bubbling for 9 h to obtain $Au_{25}(SG)_{18}$. Excess GSH was removed by using a dialysis membrane (MWCO 8000, Fisher Scientific) under gentle stirring at <10 °C for 12 h. The precipitate formed was removed with a filter (pore size 0.2 μm).

An aqueous solution of the synthesized $Au_{25}(SG)_{18}$ exhibits three absorption peaks at 1.84 eV (674 nm), 2.75 eV (451 nm), and 3.86 eV (321 nm) and an absorption onset at 1.3 eV (950 nm) (Fig. 2b). These features are in good agreement with those of $Au_{25}(SR)_{18}$ reported elsewhere.[3,36–39]

Synthesis of $Au_{38}(SG)_{24}$ and $Au_{102}(SG)_{44}$

$Au_{38}(SG)_{24}$ and $Au_{102}(SG)_{44}$ were synthesized and separated according to our previous report.[13] GSH (0.8 mmol) was added to an ice-cold aqueous solution of $HAuCl_4$ (5 mM, 40 mL) and stirred for 30 min. An ice-cold aqueous $NaBH_4$ (0.2 M, 10 mL) was added under vigorous stirring and aged for 12 h at room temperature. The solution was divided into four aliquots and each was added dropwise to methanol (18.75 mL). The precipitate formed was collected by centrifugation (13 000g, 10 min) and thoroughly rinsed with methanol and dried in a vacuum at room temperature to obtain a mixture of Au CLs.

The mixture (~10 mg) was dissolved in 1 mL aqueous glycerin (5 vol%) and separated by electrophoresis with a 16–26% gradient polyacrylamide gel under a bias voltage of 150 V in an ice-cold bath for 10 h.[40] The bands of $Au_{38}(SG)_{24}$ (migration distance: 68 mm) and $Au_{102}(SG)_{44}$ (migration distance: 56 mm) (Fig. 2a) were cut out of the gel and immersed in pure water (2 mL) in a refrigerator overnight or longer to extract the Au CLs. The obtained CL solutions were filtered (pore size, 0.2 μm) to remove the gel.

An aqueous solution of the synthesized $Au_{38}(SG)_{24}$ is characterized by five distinct absorption peaks at 1.20 eV (1033 nm),
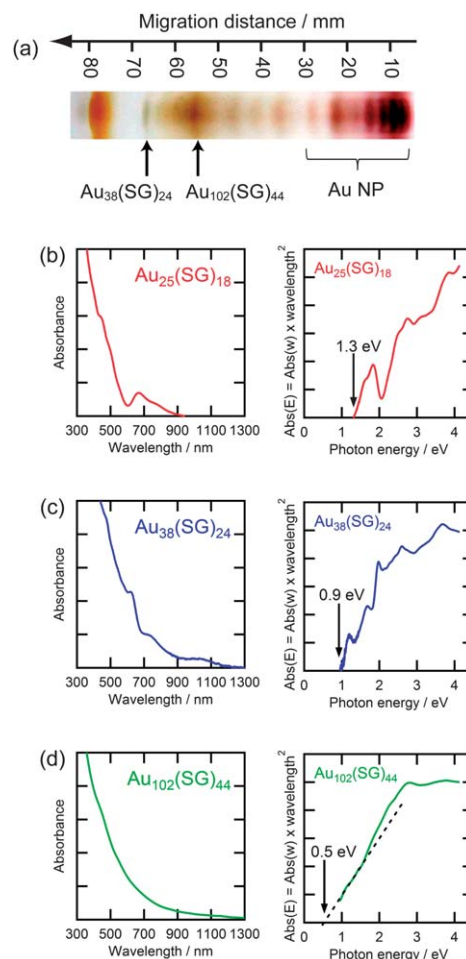
Fig. 2 (a) Electrophoretic pattern of $Au_{38}(SG)_{24}$ and $Au_{102}(SG)_{44}$. Absorption spectra of (b) $Au_{25}(SG)_{18}$, (c) $Au_{38}(SG)_{24}$ and (d) $Au_{102}(SG)_{44}$.

1.69 eV (734 nm), 1.98 eV (626 nm), 2.60 eV (477 nm), and 3.69 eV (336 nm) and the absorption onset at 0.9 eV (1380 nm) (Fig. 2c), which correspond to the features of $Au_{38}(SR)_{24}$ described in previous reports.[39,41–44] Two weak absorption peaks at 2.78 eV (446 nm) and 3.79 eV (327 nm) and an absorption onset at 0.5 eV (2480 nm) are observed for the synthesized $Au_{102}(SG)_{44}$ (Fig. 2d). These characteristics are close to those for $Au_{102}(SR)_{44}$ reported elsewhere.[39,45,46] These assignments were supported by the electrophoretic migration distance.[13]

Fabrication of $ITO/Au NP/TiO_2/Au CL$ electrodes

We fabricated two-dimensional $ITO/Au NP/TiO_2/Au CL$ (NP = nanoparticle) and $ITO/TiO_2/Au CL$ electrodes (Fig. 1b and c) as follows. A thin Au film (~10 nm thick) was vapor-deposited on a smooth ITO (indium tin oxide)-coated glass plate (Kuramoto) with vacuum deposition equipment (VPC-260F, ULVAC). The substrate was heated at 500 °C for 1 h to convert the Au film to Au NPs (Fig. 1d). The average width and height were estimated to be 42.3 ± 17.6 nm and 14.6 ± 5.4 nm, respectively, by atomic force microscopy (AFM, NanoNavi Station, Hitachi High-Tech Science). The surface coverage of Au NPs was estimated to be 2.5 × 10^{10} particles per cm^2. The ITO surface with the Au NPs and a

bare ITO surface were coated with thin TiO_2 films prepared by a spray pyrolysis method[47–49] from a 2-propanol solution of titanium diisopropoxide bis(acetylacetonate) (spray pressure was 0.12 MPa, spray time was 1 s, and calcined at 500 °C for 30 min). The thickness was measured by scanning electron microscopy (SEM, JSM-7500FA, JEOL) to be 3–100 nm for the TiO_2 films prepared from the 0.045–0.374 M solution with spraying for 1 or 3 times. The deviation for the thickness of the TiO_2 thin films prepared by this method[48,49] is about 30%.

A solution of Au CLs was cast on the ITO/Au NP/TiO_2 and ITO/TiO_2 electrodes and left for 2 h followed by thorough rinsing with pure water and drying under airflow. GSH-protected Au CLs are electrostatically bound to the anatase TiO_2 surface via their carboxyl groups at pH 2 to 6.[11] The pH values of the Au_{38} and Au_{102} solutions were adjusted to 5 with acetic acid. In the case of $Au_{25}(SG)_{18}$, acetic acid was not added because the pH value of the as-prepared solution was 3.3. The concentration of the $Au_{25}(SG)_{18}$ solution was $\sim 2 \times 10^{-5}$ M (estimated with a molar extinction coefficient of 8.8×10^3 M^{-1} cm^{-1} at 670 nm[3]). The absorbances of $Au_{38}(SG)_{24}$ and $Au_{102}(SG)_{44}$ solutions were ~ 0.4 and ~ 1.8 at 300 nm, respectively. Absorption spectra of the solutions and electrodes were measured with a spectrophotometer (V-670, JASCO). Spatial distributions of the electric field around the Au NPs were calculated on the basis of a finite-difference time-domain (FDTD) method via FDTD Solutions (Lumerical Solutions).

Photoelectrochemical measurements

Two-electrode thin layer cells were constructed as follows: a HIMILAN film (50 μm thick, DuPont-Mitsui Polychemicals) with a 0.25 cm^2 or 0.20 cm^2 window was sandwiched between the ITO/Au NP/TiO_2/Au CL or ITO/TiO_2/Au CL working electrode and a Pt-coated ITO counter electrode. The interspace between the two electrodes was filled with acetonitrile containing a 0.1 M electron donor and 0.1 M tetra-n-butylammonium perchlorate, which was deaerated by N_2. Lithium iodide or hydroquinone was employed as an electron donor. The cell was irradiated from the back of the working electrode with monochromatic light (6×10^{15} photons per cm^2 per s, full width at half maximum (fwhm) = 10 nm) using a 100 W Xe lamp (LAX-102, Asahi Spectra) through a bandpass filter (Asahi Spectra) and short-circuit photocurrents were measured with a potentiostat (1280C, Solartron).

### Quantitation of the amounts of adsorbed Au CLs

0.05 M NaOH aqueous solution (pH 12) was cast on the surface of the ITO/Au NP/TiO_2/Au CL or ITO/TiO_2/Au CL electrode and left for 4 h. The amount of the Au CLs desorbed from the electrode into the solution was determined by inductively coupled plasma mass spectrometry (SPQ9000, Hitachi High-Tech Science).

3   Results and discussion

In this work we prepared two-dimensional[48–51] ITO/Au NP/Au CL electrodes (Fig. 1b and e) to allow control of the CL–NP

spacing by changing the TiO_2 thickness. If we use a three dimensional and nanoporous system, which gives higher photocurrents, effects of the spacing and CL size cannot be separated from effects of electron and ion transport. The ITO/Au NP/TiO_2/Au_{25} electrodes exhibited larger extinction (= absorption + scattering) than the electrodes without Au NPs (Fig. 1c) in the wavelength range >600 nm due to LSPR of Au NPs (Fig. 3a). The spectrum of the ITO/TiO_2/Au_{25} does not agree with that of a Au_{25} aqueous solution (Fig. 2b) since an interference effect of the ITO and TiO_2 layers is more significant than the absorption of Au_{25}.

Consistent with our previous report,[11] the Au_{25}-modified TiO_2 electrode generated stable anodic photocurrents in response to visible and near infrared light in the presence of hydroquinone as an electron donor. The photocurrent action spectra for the electrodes with a 6 nm thick TiO_2 layer are shown
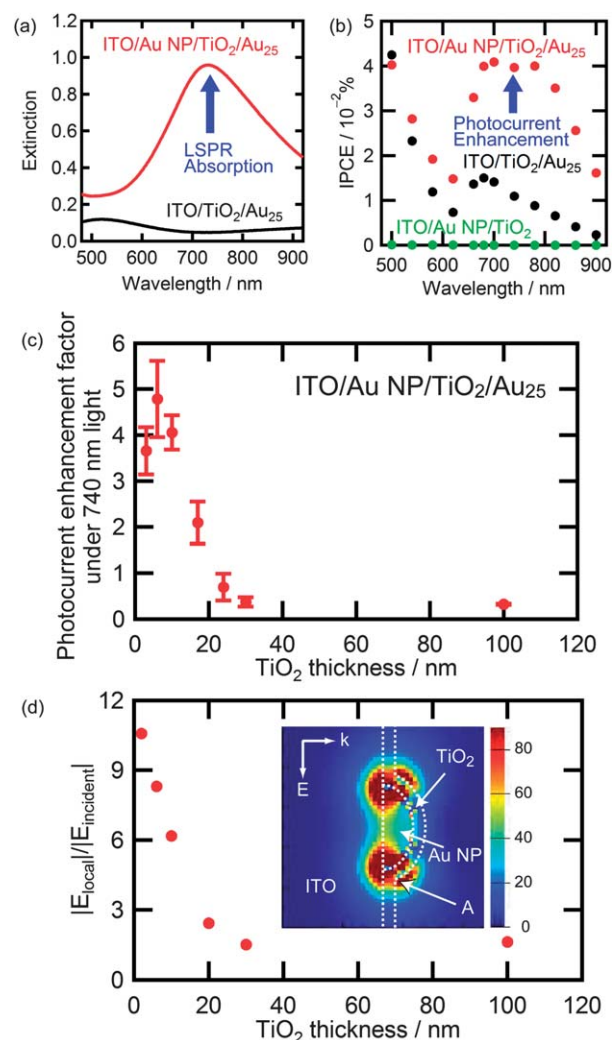
Fig. 3 (a) Absorption spectra and (b) photocurrent action spectra in the presence of hydroquinone (0.5 M) for ITO/Au NP/TiO_2(6 nm)/Au_{25}, ITO/TiO_2(6 nm)/Au_{25} and ITO/Au NP/TiO_2(6 nm) electrodes. (c) Photocurrent enhancement factor under 740 nm light and (d) the maximum localized electric field intensity at the TiO_2 surface (point A) calculated by a FDTD method, both plotted against the TiO_2 thickness. ((d), inset) Electric field distribution for a model with 6 nm thick TiO_2 under 843 nm light.

in Fig. 3b. The action spectrum of the ITO/TiO$_2$/Au$_{25}$ electrode (Fig. 3b) is in good agreement with the extinction spectrum of aqueous Au$_{25}$ (Fig. 2b). This suggests that the photocurrents generate on the basis of electron injection from Au$_{25}$ to TiO$_2$ (Fig. 1a).[11] On the other hand, the ITO/Au NP/TiO$_2$/Au$_{25}$ electrode exhibited 2–9 times as large photocurrents as that without Au NPs at 600–900 nm (Fig. 3b), at which the Au NPs exhibit intense LSPR. Ratios of the number of Au$_{25}$ CLs on the electrode with Au NPs to that without Au NPs were evaluated to be <1.4 so that we can conclude that the photocurrent enhancement is not due to the difference in the amount of the adsorbed Au$_{25}$ on the two electrodes. At wavelengths below 600 nm, where LSPR is weak or absent, the enhancement factor (*e.g.* 1.3 at 540 nm) was close to the ratio of the number of adsorbed CLs. Incidentally, photocurrents of ITO/Au NP/TiO$_2$ electrodes were negligibly small (Fig. 3b). If these currents are increased by Au CL, the photocurrents should be cathodic, although the Au CL–NP diad system exhibits anodic photocurrents as described above. These results suggest that the photocurrents are enhanced by the plasmonic Au NPs.

If the enhancement was induced by LSPR of Au NPs, the enhancement factor should increase as the spacing between the NP and the photosensitizer decreases, because the plasmonic near field intensifies.[19,48–52] When the spacing becomes too small, however, the enhancement becomes less significant.[19,48,49,51,52] So we investigated the dependence of the photocurrent enhancement on the CL-NP spacing by controlling the TiO$_2$ thickness (Fig. 3c). When the spacing was 30 nm or larger, the photocurrents in the presence of Au NPs were lower than those in the absence of the NPs. This negative effect is explained in terms of a screening effect; the extinction of NPs reduces the number of photons reaching CLs. On the other hand, when the spacing was shorter than 20 nm, the photocurrents were enhanced by the Au NPs; a positive effect exceeded the negative screening effect. The maximum enhancement factor was reached at 6 nm and seemed to decrease at the shorter spacing. These results indicate that the positive enhancement effect is due to the plasmonic near field.

We also carried out finite-difference time domain (FDTD) calculations to simulate the electric field distribution for an oblate Au hemisphere (42 nm wide and 15 nm high) coated with 6 nm thick TiO$_2$ (Fig. 3d, inset). In Fig. 3d, the electric field intensity at point A (indicated by the arrow in the inset) at the wavelength which gives the highest intensity is plotted against the TiO$_2$ thickness. The intensity increases as the TiO$_2$ thickness decreases. This behavior corresponds to that of the photocurrent enhancement in the TiO$_2$ thickness range of ≥10 nm (Fig. 3c). However, the photocurrent enhancement saturates or decreases when the thickness is <10 nm, although the electric field intensity still increases. Such suppression of enhancement is often observed for the plasmonic enhancement of fluorescence,[52] photocatalysis[19] and photocurrents of dye-sensitized solar cells.[48,49,51] In those reports, the suppression is explained in terms of energy transfer from dyes or semiconductor nanoparticles to metal NPs, which is accelerated when the spacing between them is small enough. The energy transfer should also take place in the present system, since the bandgap of TiO$_2$

(~3.2 eV) is sufficiently larger than the energy range examined (<2.5 eV) and TiO$_2$ cannot trap the energy.

We also employed Au$_{38}$ and Au$_{102}$. Their HOMO potentials are too negative to receive electrons from hydroquinone.[13] We therefore used I$^-$ as an electron donor. We have previously proven that TiO$_2$ modified with those CLs exhibits stable photocurrents in the presence of I$^-$ and that ligand exchange and etching of the CLs by I$^-$ are negligible during the photoelectrochemical measurements under deaerated conditions, on the basis of stable photocurrents and absorption spectra.[13] All Au CL-sensitized TiO$_2$ electrodes generated photocurrents under 500–900 nm monochromatic light (Fig. 4a–c, black symbols). The action spectrum of the ITO/TiO$_2$/Au$_{38}$ electrode (Fig. 4b) is rather featureless in comparison with the absorption spectrum of a Au$_{38}$ aqueous solution (Fig. 2c). This is because the absorption spectrum consists of many different electron transitions from HOMO−2, HOMO−1 and HOMO to LUMO, LUMO+1, LUMO+2 and LUMO+3 (ref. 53) and the contribution of each transition to the photocurrent is not the same.

In the case of Au$_{25}$ (Fig. 4a), the Au NPs enhanced the photocurrents in the wavelength range of 600–900 nm, as in the system with hydroquinone (Fig. 3b). Au$_{38}$-sensitized currents were also enhanced by Au NPs, and the enhancement factor (2.3 ± 0.6 at 740 nm, Fig. 4b) was slightly smaller than that for Au$_{25}$ (2.9 ± 0.5). When Au$_{102}$ was employed, however, the photocurrents were suppressed by Au NPs (Fig. 4c). We obtained similar results for TiO$_2$ layers with different thicknesses (3–10 nm). Since the electric field intensity at the TiO$_2$ surface does not depend on the CL size, the decrease in the enhancement factor with increasing CL size (Fig. 4d) is ascribed to accelerated back energy transfer from Au CLs to NPs. The energy transfer is based on the dipole–dipole interaction between a NP and a CL. Since the interaction becomes stronger as the dipole moment increases, a larger CL should be easier to transfer energy to a NP. Actually, energy transfer from
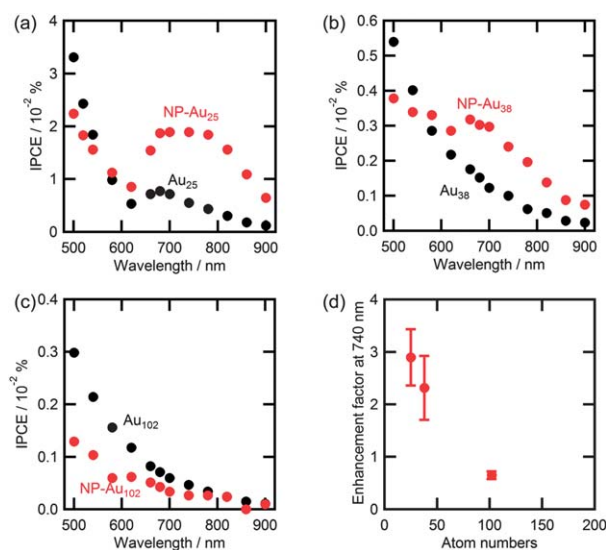
Fig. 4 Photocurrent action spectra for the ITO/Au NP/TiO$_2$(6 nm)/Au CL and ITO/TiO$_2$(6 nm)/Au CL electrodes in the presence of LiI: (a) Au$_{25}$(SG)$_{18}$, (b) Au$_{38}$(SG)$_{24}$ and (c) Au$_{102}$(SG)$_{44}$. (d) Enhancement factor of photocurrents under 740 nm light as a function of the CL size.

CdTe quantum dots to Au NPs becomes more significant as the quantum dot size increases.[54]

The plasmonic enhancement of Au CLs may be involved in the case of polydisperse Au NPs deposited photocatalytically or chemically on TiO_2, because Au CLs may also be deposited with NPs.[26,55] Notably, Kominami et al.[55] reported that photocatalytic H_2 generation from alcohol on TiO_2 modified with plasmonic Au NPs was improved by coexisting cluster-sized Au particles. Although their average size, $\sim$1.4 nm, corresponds to 100 Au atoms, CLs smaller than the average size would benefit from the plasmonic enhancement. Moreover, Kamat et al.[56] suggested that the photocatalytic activity of Ag NPs was increased by CL segments at the NP surface. This can also be explained in terms of the plasmonic enhancement of the CL-sensitized process. It is also suggested that the plasmon-induced charge separation of metal NP–TiO_2 systems would be improved in efficiencies and functionalities by introducing CLs which effectively work as a photosensitizer as well as a catalyst.

4 Conclusions

In this study, we have developed Au CL–NP diad systems on TiO_2 and enhanced the Au_{25}-sensitized processes by plasmonic near field around Au NPs. The maximum enhancement factor of $\sim$9 was reached when the CL–NP spacing was 3–10 nm. The enhancement was also observed for Au_{38}, but not for Au_{102}. Thus, performances of photovoltaics and photocatalysis based on small metal CLs would be improved by plasmonic metal NPs. We also suggest that the efficiency of the plasmon-induced charge separation of NP–semiconductor systems would be enhanced by introducing appropriate metal CLs. Diad systems with metal NPs as an antenna and metal CLs as a photosensitizer/catalyst would allow development of further sophisticated photofunctional materials and devices.

Acknowledgements

Notes and references

1 M. Zhu, C. M. Aikens, F. J. Hollander, G. C. Schatz and R. Jin, J. Am. Chem. Soc., 2008, 130, 5883.

2 C. M. Aikens, J. Phys. Chem. C, 2008, 112, 19797.

3 Y. Negishi, K. Nobusada and T. Tsukuda, J. Am. Chem. Soc., 2005, 127, 5261.

4 Z. Wu, C. Gayathri, R. R. Gil and R. Jin, J. Am. Chem. Soc., 2009, 131, 6535.

5 T. Huang and R. W. Murray, J. Phys. Chem. B, 2001, 105, 12498.

6 S. Ling, A. Beeby, S. FitzGerald, M. A. El-Sayed, T. G. Schaaff and R. L. Whetten, J. Phys. Chem. B, 2002, 106, 3410.

7 G. Ramakrishna, O. Varnavski, J. Kim, D. Lee and T. Goodson, J. Am. Chem. Soc., 2008, 130, 5032.

8 Y. Zhang, X. Cui, F. Shi and Y. Deng, Chem. Rev., 2012, 112, 2467.

9 T. Inasaki and S. Kobayashi, Electrochim. Acta, 2009, 54, 4893.

10 M. Grätzel, Acc. Chem. Res., 2009, 42, 1788.

11 N. Sakai and T. Tatsuma, Adv. Mater., 2010, 22, 3185.

12 N. Sakai, T. Ikeda, T. Teranishi and T. Tatsuma, ChemPhysChem, 2011, 12, 2415.

13 A. Kogo, N. Sakai and T. Tatsuma, Nanoscale, 2012, 4, 4217.

14 A. Kogo, N. Sakai and T. Tatsuma, Electrochem. Commun., 2010, 12, 996.

15 M. J. Hostetler, J. E. Wingate, C.-J. Zhong, J. E. Harris, R. W. Vachet, M. R. Clark, J. D. Londono, S. J. Green, J. J. Stokes, G. D. Wignall, G. L. Glish, M. D. Porter, N. D. Evans and R. W. Murray, Langmuir, 1998, 14, 17.

16 P. K. Jain, K. S. Lee, I. H. El-Sayed and M. A. El-Sayed, J. Phys. Chem. B, 2006, 110, 7238.

17 P. L. Stiles, J. A. Dieringer, N. C. Shah and R. P. Van Duyne, Annu. Rev. Anal. Chem., 2008, 1, 601.

18 J. A. Schuller, E. S. Barnard, W. Cai, Y. C. Jun, J. S. White and M. L. Brongersma, Nat. Mater., 2010, 9, 193.

19 T. Torimoto, H. Horibe, T. Kameyama, K. Okazaki, S. Ikeda, M. Matsumura, A. Ishikawa and H. Ishihara, J. Phys. Chem. Lett., 2011, 2, 2057.

20 K. Awazu, M. Fujimaki, C. Rockstuhl, J. Tominaga, H. Murakami, Y. Ohki, N. Yoshida and T. Watanabe, J. Am. Chem. Soc., 2008, 130, 1676.

21 S. Linic, P. Christopher and D. B. Ingram, Nat. Mater., 2011, 10, 911.

22 P. Wang, B. Huang, Y. Dai and M.-H. Whangbo, Phys. Chem. Chem. Phys., 2012, 14, 9813.

23 C. Wen, K. Ishikawa, M. Kishima and K. Yamada, Sol. Energy Mater. Sol. Cells, 2000, 61, 339.

24 M. Ihara, M. Kanno and S. Inoue, Physica E, 2010, 42, 2867.

25 H. A. Atwater and A. Polman, Nat. Mater., 2010, 9, 205.

26 Y. Tian and T. Tatsuma, J. Am. Chem. Soc., 2005, 127, 7632.

27 Y. Tian and T. Tatsuma, Chem. Commun., 2004, 1810.

28 T. Yamaguchi, E. Kazuma, N. Sakai and T. Tatsuma, Chem. Lett., 2012, 41, 1340.

29 E. Kowalska, R. Abe and B. Ohtani, Chem. Commun., 2009, 241.

30 H. Kominami, A. Tanaka and K. Hashimoto, Chem. Commun., 2010, 46, 1287.

31 Y. Ohko, T. Tatsuma, T. Fujii, K. Naoi, C. Niwa, Y. Kubota and A. Fujishima, Nat. Mater., 2003, 2, 29.

32 E. Kazuma and T. Tatsuma, Chem. Commun., 2012, 48, 1733.

33 I. Tanabe and T. Tatsuma, Nano Lett., 2012, 12, 5418.

34 T. Tatsuma, Bull. Chem. Soc. Jpn., 2013, 86, 1.

35 T. Tatsuma, K. Takada and T. Miyazaki, Adv. Mater., 2007, 19, 1249.

36 Y. Shichibu, Y. Negishi, H. Tsunoyama, M. Kanehara, T. Teranishi and T. Tsukuda, Small, 2007, 3, 835.

37 D. Lee, R. L. Donkers, G. L. Wang, A. S. Harper and R. W. Murray, J. Am. Chem. Soc., 2004, 126, 6193.

38 D. García-Raya, R. Madueño, M. Blázquez and T. Pineda, J. Phys. Chem. C, 2009, 113, 8756.

39 T. Tsukuda, *Bull. Chem. Soc. Jpn.*, 2012, **85**, 151.

40 K. Kimura, N. Sugimoto, S. Sato, H. Yao, Y. Negishi and T. Tsukuda, *J. Phys. Chem. C*, 2009, **113**, 14076.

41 H. Qian, Y. Zhu and R. Jin, *ACS Nano*, 2009, **3**, 3795.

42 H. Tsunoyama, P. Nickut, Y. Negishi, K. Al-Shamery, Y. Matsumoto and T. Tsukuda, *J. Phys. Chem. C*, 2007, **111**, 4153.

43 H. Qian, M. Zhu, U. N. Anderson and R. Jin, *J. Phys. Chem. A*, 2009, **113**, 4281.

44 N. K. Chaki, Y. Negishi, H. Tsunoyama, Y. Shichibu and T. Tsukuda, *J. Am. Chem. Soc.*, 2008, **130**, 8608.

45 Y. Levi-Kalisman, P. D. Jadzinsky, N. Kalisman, H. Tsunoyama, T. Tsukuda, D. A. Bushnell and R. D. Kornberg, *J. Am. Chem. Soc.*, 2011, **133**, 2976.

46 E. Hulkko, O. Lopez-Acevedo, J. Koivisto, T. Levi-Kalisman, R. D. Kornberg, M. Petterson and H. Häkkinen, *J. Am. Chem. Soc.*, 2011, **133**, 3752.

47 Y. Tachibana, K. Umekita, Y. Otsuka and S. Kuwabata, *J. Phys. D: Appl. Phys.*, 2008, **41**, 102002.

48 T. Kawawaki, Y. Takahashi and T. Tatsuma, *Nanoscale*, 2011, **3**, 2865.

49 T. Kawawaki, Y. Takahashi and T. Tatsuma, *J. Phys. Chem. C*, 2013, **117**, 5901.

50 S. D. Standridge, G. C. Schatz and J. T. Hupp, *J. Am. Chem. Soc.*, 2009, **131**, 8407.

51 T. Kameyama, Y. Ohno, K. Okazaki, T. Uematsu, S. Kuwabata and T. Torimoto, *J. Photochem. Photobiol., A*, 2011, **221**, 244.

52 P. Anger, P. Bharadwaj and L. Novotny, *Phys. Rev. Lett.*, 2006, **96**, 113002.

53 O. Lopez-Acevedo, H. Tsunoyama, T. Tsukuda, H. Häkkinen and C. M. Aikens, *J. Am. Chem. Soc.*, 2010, **132**, 8210.

54 X. Zhang, C. A. Marocico, M. Lunz, V. A. Gerard, Y. K. Gun'ko, V. Lesnyak, N. Gaponik, A. S. Susha, A. L. Rogach and A. L. Bradley, *ACS Nano*, 2012, **6**, 9283.

55 A. Tanaka, S. Sakaguchi, K. Hashimoto and H. Kominami, *Catal. Sci. Technol.*, 2012, **2**, 907.

56 W. T. Chen, Y. J. Hsu and P. V. Kamat, *J. Phys. Chem. Lett.*, 2012, **3**, 2493.